Halogens as tracers of protosolar nebula material in comet 67P/Churyumov-Gerasimenko

Frederik Dhooghe[1]* , Johan De Keyser[1,2], Kathrin Altwegg[3,4], Christelle Briois[5], Hans Balsiger[3], Jean-Jacques Berthelier[6], Ursina Calmonte[3], Gaël Cessateur[1], Michael R. Combi[7], Eddy Equeter[1], Björn Fiethe[8], Nicolas Fray[9], Stephen Fuselier[10,11], Sébastien Gasc[3], Andrew Gibbons[1,12], Tamas Gombosi[7], Herbert Gunell[1], Myrtha Hässig[3,10], Martin Hilchenbach[13], Léna Le Roy[4], Romain Maggiolo[1], Urs Mall[13], Bernard Marty[14], Eddy Neefs[1], Henri Rème[15,16], Martin Rubin[3], Thierry Sémon[3], Chia-Yu Tzou[3], Peter Wurz[3,4]

[1] *Royal Belgian Institute for Space Aeronomy, BIRA-IASB, Ringlaan 3, B-1180 Brussels, Belgium*
[2] *Center for mathematical Plasma Astrophysics, KULeuven, Celestijnenlaan 200B, B-3001 Heverlee, Belgium*
[3] *Physikalisches Institut, University of Bern, Sidlerstr. 5, CH-3012 Bern, Switzerland*
[4] *Center for Space and Habitability, University of Bern, Sidlerstr. 5, CH-3012 Bern, Switzerland*
[5] *Laboratoire de Physique et Chimie de l'Environnement et de l'Espace (LPC2E), UMR CNRS 7328, Université d'Orléans, France*
[6] *LATMOS/IPSL-CNRS-UPMC-UVSQ, 4 Avenue de Neptune F-94100, Saint-Maur, France*
[7] *Department of Climate and Space Sciences and Engineering, University of Michigan, 2455 Hayward, Ann Arbor, MI 48109, USA*
[8] *Institute of Computer and Network Engineering (IDA), TU Braunschweig, Hans-Sommer-Straße 66, D-38106 Braunschweig, Germany*
[9] *Laboratoire Interuniversitaire des Systèmes Atmosphériques (LISA), UMR CNRS 7583, Université Paris-Est Créteil (UPEC), Université Paris Diderot (UPD)*
[10] *Space Science Directorate, Southwest Research Institute, 6220 Culebra Rd., San Antonio, TX 78228, USA*
[11] *University of Texas at San Antonio, San Antonio, TX, 78228, USA*
[12] *Service de Chimie Quantique et Photophysique, Université Libre de Bruxelles, 50 Avenue F. Roosevelt, B-1050 Brussels, Belgium*
[13] *Max-Planck-Institut für Sonnensystemforschung, Justus-von-Liebig-Weg 3, 37077 Göttingen, Germany*
[14] *Centre de Rech. Pétrographiques & Géochimiques, CRPG-CNRS, Univ. Lorraine, 15 rue N. D. des Pauvres, BP 20, 54501 Vandoeuvre lès Nancy, France*
[15] *Université de Toulouse; UPS-OMP; IRAP, Toulouse, France*
[16] *Institut de Recherches en Astrophysique et Planétologie, CNRS-IRAP; 9 Avenue du Colonel Roche, BP 44346, F-31028 Toulouse Cedex 4, France*

ABSTRACT

We report the first *in situ* detection of halogens in a cometary coma, that of 67P/Churyumov-Gerasimenko. Neutral gas mass spectra collected by the European Space AgencyâĂŹs Rosetta spacecraft during four periods of interest from the first comet encounter up to perihelion indicate that the main halogen-bearing compounds are HF, HCl and HBr. The bulk elemental abundances relative to oxygen are ~8.9×10^{-5} for F/O, ~1.2×10^{-4} for Cl/O, and ~2.5×10^{-6} for Br/O, for the volatile fraction of the comet. The cometary isotopic ratios for $^{37}Cl/^{35}Cl$ and $^{81}Br/^{79}Br$ match the solar system values within the error margins. The observations point to an origin of the hydrogen halides in molecular cloud chemistry, with frozen hydrogen halides on dust grains, and a subsequent incorporation into comets as the cloud condensed and the solar system formed.

Key words: comets:general – comets:individual:67P/Churyumov-Gerasimenko – composition

1 INTRODUCTION

While molecular clouds evolve from diffuse to dense and ultimately protostellar clouds, the halogens that initially are
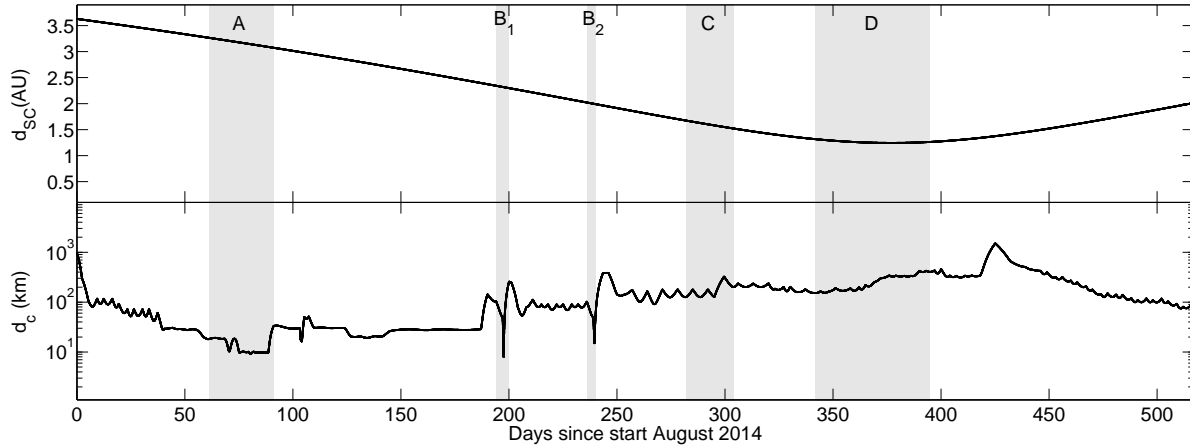
* E-mail: frederik.dhooghe@aeronomie.be

Figure 1. Sun-comet and comet-spacecraft distance for the periods of interest. The plot covers 1/8/2014 to 31/12/2015. The shaded areas indicate the periods (A) close to the comet, 1–31/10/2014, (B1 and B2) the close flybys on 14/2/2015 and on 28/3/2015, (C) post-equinox between 10/5/2015 and 1/6/2015, and (D) around perihelion between 9/7/2015 and 31/8/2015.

present in atomic form become bound in hydrogen halides. Atomic fluorine in diffuse molecular clouds reacts exothermically with the abundant H_2 and readily forms HF. The reaction of atomic chlorine and bromine with H_2 forming HCl and HBr is endothermic but still occurs easily in dense molecular clouds where free energy is available in the form of thermal energy or photons (Neufeld & Wolfire 2009). Therefore, the principal reservoirs of halogens in protostellar clouds are thought to be the hydrogen halides. This was suggested for HCl by Jura (1974) and Dalgarno et al. (1974). Astronomical detection of HCl in such clouds indicates that it is strongly depleted in the gas phase (Blake et al. 1985), which suggests that HCl is frozen out on grains in these cold environments (Peng et al. 2010; Emprechtinger et al. 2012). Kama et al. (2015) presented the first gas-grain chemical model for chlorine. Using data of various chlorine species from the Herschel Space Observatory and from the Caltech Submillimeter Observatory, they estimate that in protostellar cores at least 90% of the full chlorine inventory is locked in HCl ice. HF has been detected in diffuse clouds only in absorption spectra (Neufeld et al. 2010), similarly indicating a depletion. Very little is known about other hydrogen halides (HBr, HI).

Under the hypothesis that comets would contain pristine protostellar material, they would be prime candidates to provide information about halogens in such clouds. Bockelée-Morvan et al. (2014) measured the HF/H_2O ratio in the coma of comet C/2009 P1 (Garradd) with marginal significance to be $(1.8 \pm 0.5) \times 10^{-4}$. Attempts to obtain HCl/H_2O have resulted in upper limits of 2.2×10^{-4} for C/2009 P1 (Garradd) and 1.1×10^{-4} for 103P/Hartley 2, the former being an Oort cloud comet and the latter a Jupiter-family comet, both suggesting a HCl/H_2O depletion. As these upper limits are on the order of the solar values, a clear measurement of the halogen abundances in comets is needed to relate comets to other solar system bodies in order to trace back their history.

2   DETECTION OF HALOGEN-BEARING COMPOUNDS

The European Space Agency's Rosetta mission to 67P/Churyumov-Gerasimenko (67P/C-G) offered an unprecedented opportunity to examine a comet up close. The Double Focusing Mass Spectrometer (DFMS) of ROSINA, the Rosetta Orbiter Spectrometer for Ion and Neutral Analysis (Balsiger et al. 2007), is the instrument of choice for examining the comet's volatile inventory *in situ* (Le Roy et al. 2015). We have studied the halogen-bearing compounds in the coma with DFMS on 67P/C-G's inbound journey during four periods, while the gas production increased towards perihelion and as the latitude of the subsolar point on the comet moved from the northern to the southern hemisphere.

2.1   DFMS operating principle

The DFMS mass spectrometer was operated both in neutral and ion mode. Here, we use data collected in neutral mode in which only neutral cometary gas is detected, while coma ions cannot reach the detector (Calmonte et al. 2016). A fraction of the neutral gas is ionized and/or fragmented by electron impact ionization in the ion source. Only ion fragments in a narrow range around a certain commanded mass-over-charge ratio m/Z pass through the analyzer and impact on a microchannel plate (MCP), creating an electron avalanche that is recorded by a Linear Electron Detector Array chip (LEDA) with two rows of 512 pixels each. The data are obtained as Analog-to-Digital Converter (ADC) counts as a function of LEDA pixel number. The instrument is commanded to scan over a sequence of different m/Z values. A well-established methodology, as described in detail in Le Roy et al. (2015), is used to convert the raw DFMS data into fragment ion intensity as a function of m/Z.

2.2 Time periods of interest

The most significant fluxes of coma neutrals, including halogen-bearing gases, are observed when the spacecraft is close to the comet and/or when the comet is active (close to perihelion). High mass resolution DFMS data with sufficient signal-to-noise ratio have been obtained during the comet's inbound journey towards perihelion. Special emphasis is given to the time periods indicated in Fig. 1: (A) the 10 km orbit period when *in situ* neutral densities were obtained with high signal-to-noise ratio, (B1 and B2) the close flybys at 8 km and 13 km, (C) the period between equinox and perihelion in May 2015 when the southern hemisphere became the dominant gas source, and (D) the period around perihelion when comet activity ensured significant flux despite Rosetta's larger distance from the nucleus. We have eliminated all data during and shortly after significant spacecraft attitude changes which might lead to spacecraft outgassing (Schläppi et al. 2010), as well as times when the instrument was not pointing at the comet centre to within 5°. These time periods cover all possible latitudes, longitudes, comet-spacecraft distances, and comet-sun distances.

2.3 Fragments of halogen-bearing compounds

Because of the fragmentation of molecules in the DFMS ion source, hydrogen halides can be detected in principle in the form of the singly charged fragmentation products F, HF, ^{35}Cl and ^{37}Cl, H^{35}Cl and H^{37}Cl, ^{79}Br and ^{81}Br, and H^{79}Br and H^{81}Br; we did not detect any iodine. The mass spectra shown in Fig. 2 demonstrate that the signal was sufficiently strong to detect halogen-bearing species in 67P's coma for the first time.

Fragment ion species are detected in the form of peaks with a specific shape. To determine the number of fragment ions registered by the detector, a peak fitting algorithm is used that approximates the mass peaks by a sum of two co-centered Gaussians (see, e.g. De Keyser et al. 2015), without any *a priori* knowledge of the identity of the ions. Despite the high mass resolution, DFMS spectra can be hard to interpret because of the overlapping of mass peaks. If the peaks belong to species with a comparable abundance, disentangling them with the peak fitting process is still possible, depending on the magnitude of the mass difference between the species. However, reliably distinguishing the contribution of a low abundance species superposed on a high abundance peak can become difficult, if not impossible.

As shown in Table 1, at m/Z = 19 u/e and 20 u/e the abundant water-related fragment ions ^{18}OH and H$_2^{18}$O can overlap F and HF, respectively. They can even completely obscure them at times when the water flux is high. An example can be seen for m/Z = 20 u/e in Fig. 2 (top panel). For ^{35}Cl and H^{35}Cl at 35 u/e and 36 u/e, there is an overlap with the sulphur-bearing species H^{34}S and H$_2^{34}$S, respectively. At m/Z = 36 u/e, also another overlapping species, ^{36}Ar, is present, as reported by Balsiger et al. (2015) and shown in Fig. 2 (middle panel). H^{37}Cl cannot be determined accurately because of its small mass difference with doubly charged CS$_2$. Although it is in principle possible to detect singly charged CS$_2$ and to assess the amount of doubly charged ions if one knows the fragmentation pattern, this is not very precise when doubly charged CS$_2$ outnum-
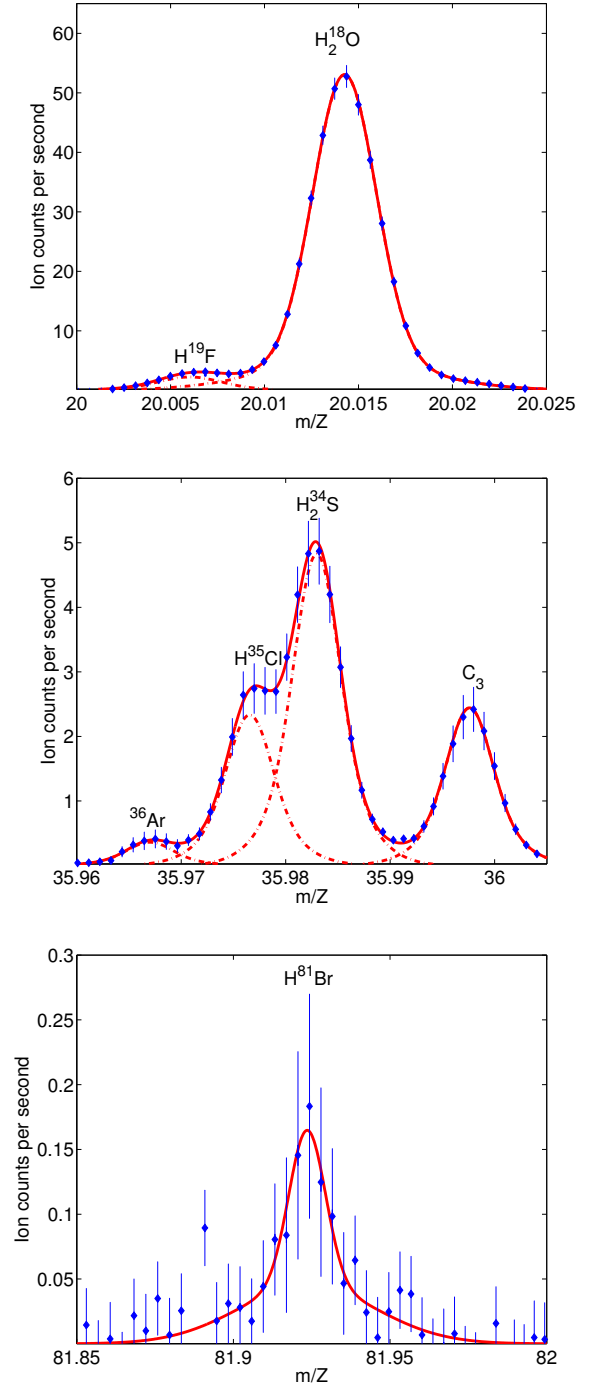

Figure 2. DFMS mass spectra showing HF, H^{35}Cl, and H^{81}Br. The spectra are from 23/10/2014 at mass-over-charge ratio m/Z = 20 u/e (08:35:32 UTC), 36 u/e (12:50:47 UTC) and 82 u/e (19:40:57 UTC). Error bars indicate the Poisson uncertainty.

bers H^{37}Cl, and also because the time difference of almost 20 minutes between the measurement of doubly and singly charged CS$_2$ at 38 and 76 u/e makes it difficult to reliably infer the CS$_2$ abundance at the moment when m/Z = 38 u/e is measured. At m/Z = 79, 80, 81, and 82 u/e bromine-bearing species can be found and there are no overlap issues; an example is given for m/Z = 82 u/e in Fig. 2 (bottom panel).

Table 1. Halogen and hydrogen halide fragment ions and interfering species. The table lists the commanded mass-over-charge ratio, the halogen-bearing fragment ions (with their mass-over-charge), and the interfering species (with mass-over-charge difference). Note that the CS_2 ion near $m/Z = 38$ is doubly charged.

Commanded mass	Interfering species	$\Delta m/Z$ (u/e)	Main species	m/Z (u/e)	Interfering species	$\Delta m/Z$ (u/e)
19			^{19}F	18.9984	^{18}OH	+0.0086
20			H^{19}F	20.0062	H$_2^{18}$O	+0.0086
35			^{35}Cl	34.9689	H^{34}S	+0.0068
36	^{36}Ar	−0.0092	H^{35}Cl	35.9767	H$_2^{34}$S	+0.0068
37			^{37}Cl	36.9659		
38	CS_2	−0.0017	H^{37}Cl	37.9737		
79			^{79}Br	78.9183		
80			H^{79}Br	79.9262		
81			^{81}Br	80.9163		
82			H^{81}Br	81.9241		

The detection system uncertainties on individual measurement points in a given mass spectrum depend on random errors (thermal fluctuations in the LEDA, noise in ADC conversion). The magnitude of these random errors can be estimated from the noise in the spectrum. Possible systematic errors (e.g. uneven aging of the MCP) have been corrected for (Le Roy et al. 2015). Integration below the fitted peak gives the number ν_Y of fragment ions Y that hit the detector during the data collection time Δt (typically 20 s); the relative uncertainty on ν_Y is significantly smaller than the relative uncertainties on the individual pixel measurements as the random errors partially cancel. As a result, the outcome is fairly precise. This detection system related uncertainty, however, is usually (much) smaller than the uncertainty $\sqrt{\nu_Y}$ due to the Poisson counting statistics. In particular for the bromine-bearing species the Poisson uncertainty is large because of their low abundances.

3   HALOGEN ABUNDANCES IN THE COMA

We now present quantitative estimates of the neutral halogen abundances in the coma of 67P. After introducing the methodology, we discuss the identity of the parent molecules and the elemental abundances of the halogen-bearing species.

3.1   Neutral abundances

The abundance n_X of a specific neutral species X can be inferred from a detected fragment ion Y using

$$n_X = \frac{aC_Y}{U_X V_Y f_{X \to Y}} \tag{1}$$

with $C_Y = c_Y − b_Y$, where $c_Y = \nu_Y/\Delta t$ denotes the integrated count rate for ion Y (corrected for instrument gain), b_Y is the integrated spacecraft background count rate for Y, U_X is the ionization efficiency for neutral X, V_Y is a factor taking into account ion-dependent instrument effects for Y, $f_{X \to Y}$ is the fraction of Y among all fragmentation products of neutral X, and $a = 1.83 \times 10^{-16}$ s is an instrument constant taking into account the detection geometry and other instrument characteristics. Very often $S_{X−Y} = U_X V_Y$ is called the sensitivity

factor. Omitting any possible systematic errors due to inaccurate sensitivities or fragmentation patterns, the relative uncertainty on n_X is the same as the one on C_Y.

Even after ten years in space, the Rosetta spacecraft is still outgassing (Schläppi et al. 2010) so that the DFMS spectra show contributions from this polluting background gas. This background has been characterized using peak fitting on mass spectra from 2nd August 2014, when Rosetta was still far from the comet (~900 km) and the comet was relatively far away from the Sun (~3.5 au). For a given fragment ion Y, the spacecraft background can significantly contribute to the integrated count rate: c_Y and b_Y may be of comparable magnitude, hence an accurate background correction is needed. A background correction was performed for HF and HCl; HBr was never detected in the background spectra.

Because HF, HCl and HBr are highly corrosive compounds, the sensitivities and fragmentation patterns for these species have not been determined experimentally with the twin instrument in the calibration facility. The instrument sensitivities for HF, F, HCl, Cl, HBr and Br have been calculated using literature data on electron ionization cross sections for these compounds from Vinodkumar et al. (2010), together with the known mass/charge dependent transmission and detection efficiencies for the fragmentation products in DFMS. The following sensitivity values were used: $S_{F−F} = 9.75 \times 10^{-20}$ cm^3, $S_{HF−HF} = S_{HF−F} = 1.63 \times 10^{-19}$ cm^3, $S_{Cl−Cl} = 2.45 \times 10^{-19}$ cm^3, $S_{HCl−HCl} = S_{HCl−Cl} = 2.58 \times 10^{-19}$ cm^3, $S_{Br−Br} = 5.66 \times 10^{-19}$ cm^3, and $S_{HBr−HBr} = S_{HBr−Br} = 5.76 \times 10^{-19}$ cm^3; these numbers are believed to be precise within a factor of 2 (Calmonte et al. 2016). The same values have been used for all corresponding isotopes.

Time profiles of the neutral abundances have been assembled from the analysis of the individual spectra. This is illustrated for period (A) in Fig. 3. The figure shows how the halogen halide and the water abundances from DFMS, as well as the total neutral gas number density from the COmet Pressure Sensor (COPS), which is also part of ROSINA (Balsiger et al. 2007), vary more or less in sync. Most of the time, DFMS with its $20° \times 20°$ field of view in neutral mode captures gas originating essentially from all over the visible illuminated surface (Bieler et al. 2015) (except when the spacecraft is very close to the comet and/or when there is significant off-pointing). The observed density variations reflect the size of this surface as seen from Rosetta while the comet rotates. It is therefore not surprising that H_2O and the hydrogen halides vary in phase, showing that the halides are of cometary origin. Note, however, that the hydrogen halide to water ratio does not remain constant.

To correlate the abundances of two neutral species, one has to interpolate the respective time profiles in time: DFMS scans the entire mass range by stepping through all possible commanded m/Z values, so that abundances for different neutral species are derived from spectra taken at different times. Such interpolation may introduce unwanted inaccuracies. We therefore interpolate the abundances of the species that is measured most frequently onto the time scale of the species measured less frequently (only in this manner does one obtain a set of statistically independent ratios). Interpolation is only allowed if the time difference between successive measurements for the neutral to be interpolated is
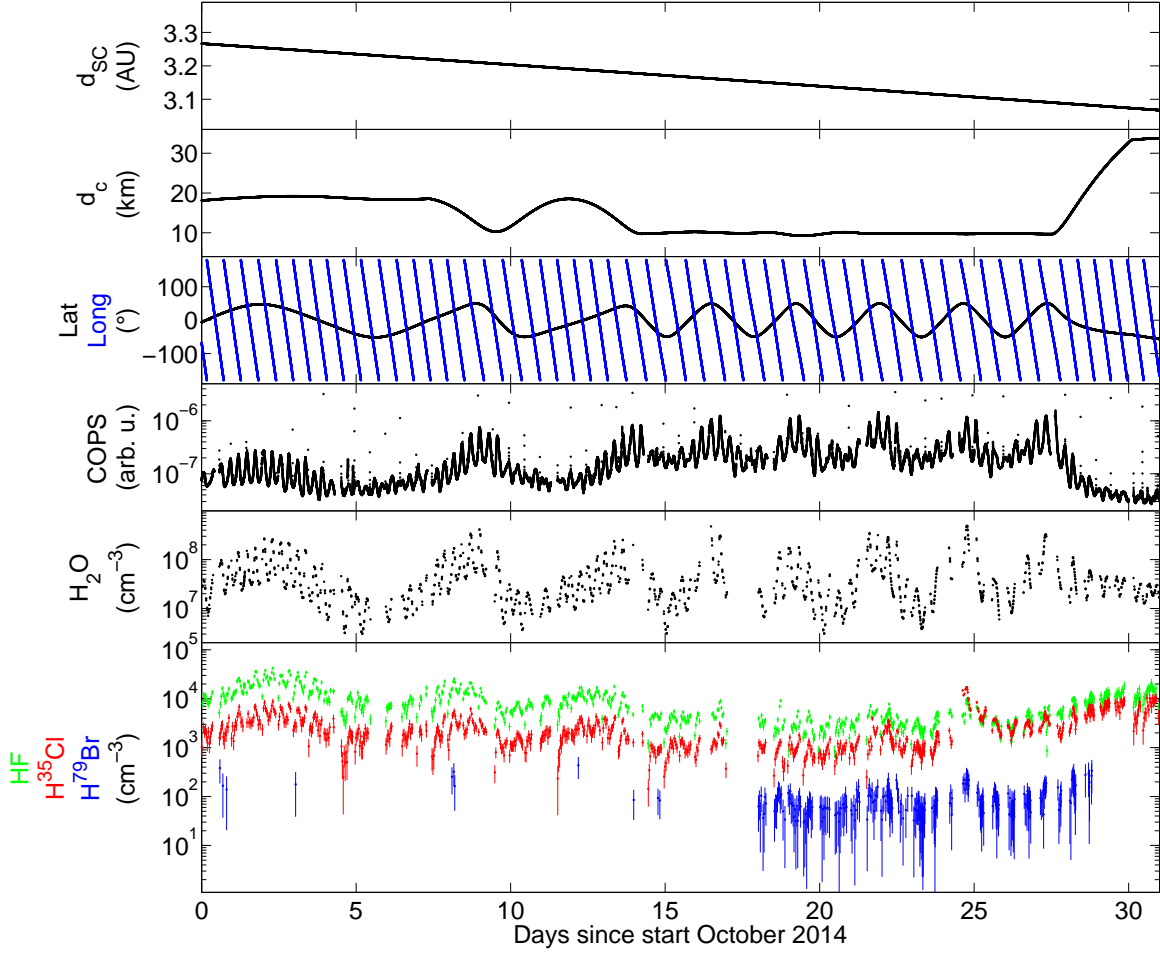
Figure 3. Hydrogen halide time variability in October 2014. The figure plots the comet's heliocentric distance, Rosetta's cometocentric distance and its latitude and longitude, the neutral coma number density from COPS, and the abundances of H_2O and of HF, $H^{35}Cl$, and $H^{79}Br$ from DFMS. Error bars reflect the Poisson error; systematic errors dominated by the uncertainty on the sensitivities are not indicated here as they would lead to vertical offsets without changing the time variability pattern.

less than 1 hour (~1/12th of the comet's rotation period). Uncertainties on the interpolated values are obtained using error propagation.

3.2 Parent molecule identity

The identity and quantity of the fragment ions detected by DFMS are linked to the identities and abundances of the neutrals that entered the instrument. An important element for determining the neutral composition are the fragmentation patterns for each neutral species. Table 2 summarizes the fragmentation patterns as given by the National Institute of Standards and Technology (NIST). It should be noted that the fragmentation patterns depend on the electron energies (70 eV for NIST, 45 eV in DFMS) and the design of the ion source (filament geometry and electric potentials). Note that the doubly charged ions are ignored, and that the fragmentation patterns are considered to be essentially identical for all isotopes.

As illustrated in Fig. 4, the DFMS data show roughly constant proportions (within the error margins) between the hydrogen halide fragment ions and the corresponding halogen ions: C_F/C_{HF} = 0.16±0.01, C_{Cl}/C_{HCl} = 0.37±0.02, and C_{Br}/C_{HBr} = 0.75±0.05. One has, in general, for halogen halide HX

$$\frac{C_X}{C_{HX}} = \frac{n_X S_{X-X} f_{X \to X} + n_{HX} S_{HX-X} f_{HX \to X}}{n_{HX} S_{HX-HX} f_{HX \to HX}} \qquad (2)$$

where C_X and C_{HX} represent the fragment ion abundances corrected for the background, and n_X and n_{HX} the neutral gas abundances of the halogen and the hydrogen halide. One can simplify this relation by assuming that the DFMS sensitivities S_{X-X}, S_{HX-X} and S_{HX-HX} do not differ much, which is plausible given the comparable masses of the corresponding halogen and hydrogen halide. Given the absence of other halogen-bearing species with a significant abundance in the DFMS mass spectra, only two alternatives remain open.
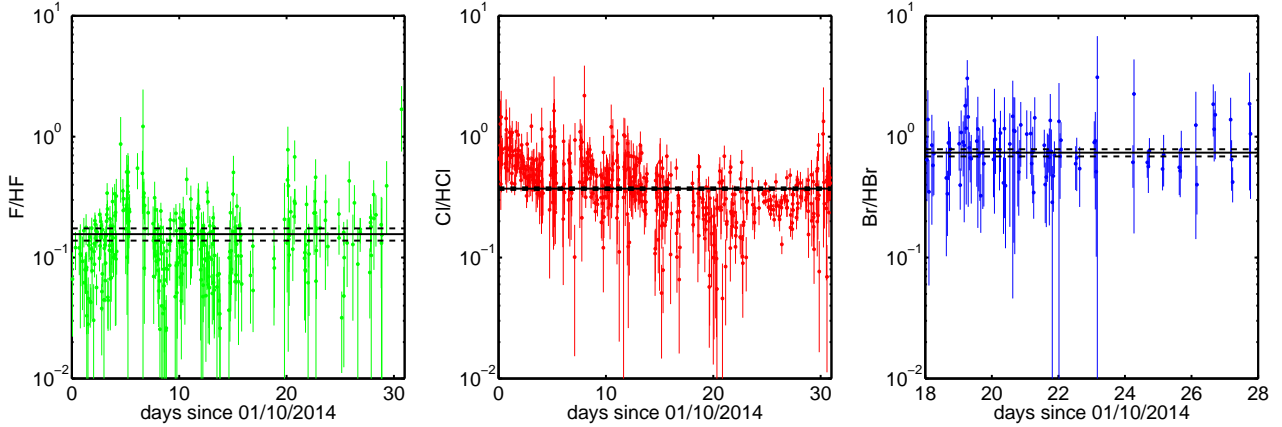
A first option is to assume that the only parent is HX,

Figure 4. Ratios between halogen fragment ions and hydrogen halide fragment ions observed by DFMS. The solid lines indicate the weighted average, while the dashed lines represent the 1σ uncertainty on the average. The ratios appear to be fairly constant within the measurement error margins. The error margins reflect the Poisson uncertainty. Uncertainties on the sensitivities largely cancel out when considering the fragment ratios. Additional uncertainty due to the interpolation of the measurements to a common time scale has not been included in the error bars, but such errors are limited since measurements of a halogen and the corresponding hydrogen halide usually are performed successively.

Table 2. Hydrogen halide fragmentation patterns from the NIST database, and from DFMS if one assumes that the hydrogen halides are the only parent neutrals.

Parent		Fragment	NIST Fraction	DFMS Fraction
F	$\rightarrow$	F^+	1.00	1.00
HF	$\rightarrow$	HF^+	not given	0.87 ± 0.01
HF	$\rightarrow$	F^+	not given	0.13 ± 0.01
Cl	$\rightarrow$	Cl^+	1.00	1.00
HCl	$\rightarrow$	HCl^+	0.85	0.73 ± 0.01
HCl	$\rightarrow$	Cl^+	0.15	0.27 ± 0.01
Br	$\rightarrow$	Br^+	1.00	1.00
HBr	$\rightarrow$	HBr^+	0.72	0.57 ± 0.02
HBr	$\rightarrow$	Br^+	0.28	0.43 ± 0.02

i.e. that $n_X \ll n_{HX}$. One then finds

$$\frac{C_X}{C_{HX}} = \frac{f_{HX \rightarrow X}}{f_{HX \rightarrow HX}}.$$

Since the neutral hydrogen halide has only two fragmentation channels, $f_{HX \rightarrow X} = 1 - f_{HX \rightarrow HX}$, so that one can rewrite the above expression as

$$f_{HX \rightarrow HX} = \frac{1}{1 + C_X/C_{HX}}.$$

From this we have computed the fragmentation fractions mentioned in the last column of Table 2. These do differ from the NIST ones, which is not surprising. The trend of decreasing proportion of the HX ion with increasing mass is expected.

A second option is to allow the coma to contain both the halogen and the hydrogen halide. From Eq. 2 one can then infer

$$\frac{n_X}{n_{HX}} = \frac{(C_X/C_{HX})f_{HX \rightarrow HX} - f_{HX \rightarrow X}}{f_{X \rightarrow X}}.$$

Assuming that the NIST fragmentation fractions are applicable to DFMS, we then find that the ratio of neutral Cl to HCl in the coma would be 0.16±0.02 and the ratio of Br over HBr would be 0.26±0.04 (where the error margins do not include the uncertainty stemming from the sensitivity estimates). No similar calculation can be done for F and HF since NIST does not provide the fragmentation pattern. Since the measured proportion of the fragments is fairly constant, the ratio of the neutral halogen and hydrogen halide must be rather constant as well.

All in all, the conclusion is that the hydrogen halides must be the major parent molecules, while we cannot exclude a limited admixture of atomic halogen in the coma gas.

3.3   Halogen to oxygen ratios

The hydrogen halide abundances relative to H_2O have been used in Bockelée-Morvan et al. (2014) to approximate the halogen-to-oxygen element ratios. Fig. 5 compares the hydrogen halide abundances to those of water for period A (1–24 October 2014). Note that the error bars on the water densities are almost invisibly small because of the high counting statistics. As already mentioned before, the HF, HCl, and HBr densities vary in sync with those of water, but do not scale linearly with those of water. Exponential curve fitting indicates that $n_{H_2O} \propto (n_{H_2O})^\eta$ with $\eta = 0.55 \pm 0.01$, 0.49 ± 0.02, and 0.40 ± 0.08, for HF, HCl, and HBr, respectively, showing that these species are not simply released with water. In a companion paper, De Keyser et al. (2017, this issue) examine the release process in more detail.

The H_2O abundance is a good proxy for the elemental O abundance, except at times when H_2O is not the dominant oxygen-bearing volatile (Hässig et al. 2015). We infer the elemental O abundance in the coma from the abundances of H_2O, CO_2, CO and O_2, and determine the hydrogen halide abundances in the gas coma relative to oxy-
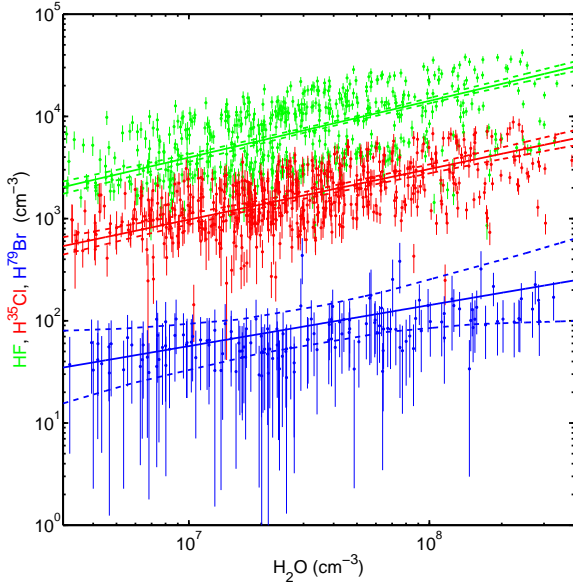
Figure 5. Hydrogen halide abundances relative to water. While the hydrogen halide densities vary with that of water, they are not linearly proportional. The error margins reflect the Poisson uncertainties. Uncertainties on the sensitivities would systematically shift the curves somewhat, without altering their slope. Additional uncertainty due to the interpolation of the measurements to a common time scale has not been included in the error bars, but such errors are limited as care has been taken to use hydrogen halide and water abundances acquired with minimal time delay. The measurements are from period A (1–24/10/2014).

gen from F/O = HF/O, Cl/O = (H^{35}Cl + H^{37}Cl)/O, and Br/O = (H^{79}Br + H^{81}Br)/O.

The hydrogen halide densities vary with the total gas production of the comet as a result of changes in the illumination conditions and a possible variability over the comet surface, all conditions dictated by comet-Sun distance, latitude and longitude of the subsolar point on the comet, and the relative position of Rosetta relative to the comet and the Sun. To compensate for these effects, we consider elemental abundance ratios of the halogens relative to oxygen, the latter reflecting the neutral gas production. The number densities of the hydrogen halides also vary inversely with the square of the distance, r^2, as long as no source or loss processes are involved.

De Keyser et al. (2017, this issue) argue that hydrogen halide sublimation may occur not only at the comet surface, but also on dust grains in the inner coma. They explain the observed halogen abundance variations near the nucleus in terms of the sublimation of halogen-enriched water ice mantles on refractory grains. Given the sublimation of the hydrogen halides close to the nucleus, their abundances are best determined at a ~200 km distance from the nucleus or more; loss processes matter only farther out in the coma, beyond 2000 km. Therefore, $r^2 n_F$, $r^2 n_{Cl}$, and $r^2 n_O$, as well as the ratios F/O and Cl/O, should remain constant in the range ~200–2000 km. Consequently, the bulk composition has been identified based on periods (C) and (D) when Rosetta was mostly between 200 and 500 km from the comet. Also, these were the periods upon approach to and around perihelion, when the gas production was highest and when the south-

ern hemisphere became exposed to sunlight, so that one can expect a larger contribution of unprocessed bulk material from the highly active southern hemisphere. For these periods, F/O varies between $(0.2 - 4) \times 10^{-4}$ and Cl/O between $(2 - 5) \times 10^{-4}$ with a weighted average bulk value of 8.9×10^{-5} for F/O and 1.2×10^{-4} for Cl/O. Since there are bromine measurements only close to the comet as count rates are too low farther out, we rely on data from period (A). For Br/O the range is $(1 - 7) \times 10^{-6}$ with a weighted average of 2.5×10^{-6}, which can be considered as a lower bound for the bulk composition. If the hydrogen halides indeed are the major halogen-bearing species, the ratios given above are good proxies for the halogen-to-oxygen ratios. The ratios given above are subject to a systematic error that stems largely from the uncertainties on the sensitivities, believed to be within a factor of 2 (Calmonte et al. 2016).

This composition is compared to that of other objects in Table 3. The F/O value for 67P/C-G is, within the uncertainty margins, quite similar to the solar system value inferred from the present-day solar composition and a model of solar evolution (Lodders 2010), and to the values found in C/2009 P1 Garradd (volatiles), CI chondrites (refractory material), and sunspots. The terrestrial F/O ratio is, however, significantly lower. The Cl/O ratio is similarly comparable to all other values, except the terrestrial one. Very little is known about Br/O. These halogen-to-oxygen ratios are compatible with the hypothesis that all halogens were locked up in the form of hydrogen halides on presolar grains and were incorporated in the comet when it was formed.

The Cl/F ratio tends to fluctuate around 1.7 (average for periods C and D, reflecting the bulk composition, varying between 0.5 and 7.0). The uncertainty on this ratio is dominated by the systematic errors on the sensitivities; by considering the ratio, these may partially cancel. This bulk Cl/F value is comparable to the upper limit of 1.2 ± 0.4 for comet C/2009 P1 (Garradd) from Bockelée-Morvan et al. (2014). A comparison to solar and meteorite ratios is difficult because these address the total abundance ratio and that of refractory material, respectively, rather than the volatile material only. In addition, meteorite ratios show a strong heterogeneity within a sample depending on mineralogical composition, differences among meteorites, and possible alteration due to volatile loss after landing on Earth. Solar and chondritic Cl/F are typically around 6 or more (Lodders 2010; Ménard et al. 2013). Note that this corresponds to the upper end of the range observed in 67P/C-G. For the ratios Br/F and Br/Cl involving bromine, values of 0.04 (between 0.02–0.10) and 0.08 (0.02–0.20), respectively, are found (average and ranges for part of period A). A comparison is even harder due to the absence of measurements in comets. In chondrites the Br/Cl ratio is around 0.002 (Lodders 2010), for Martian rocks and meteorites it is 0.002–0.05 (Cartwright et al. 2013; Squyres et al. 2012), and for Earth with considerable processing it goes up even higher (Allègre et al. 2001).

4 ISOTOPIC RATIOS

Isotopic ratios can be obtained accurately since fragmentation in the ion source and instrument sensitivity are essentially the same for both isotopes (all isotopic measurements

Table 3. Comparison of halogen/oxygen ratios (range and average) to various objects

	67P coma	Other comas	Early Sun	HII regions	Sun	Chondrites	Earth
F/O ($\times 10^{-4}$)	0.2 − 4 (0.89)	1.8 ± 0.5[a]	0.51 ± 0.12[d]		$0.7^{+0.7}_{-0.3}$ [f]	1.1 ± 0.2[h]	0.16 ± 0.02[i]
Cl/O ($\times 10^{-4}$)	2 − 5 (1.2)	< 8.0[b] < 2.2[a] < 1.1[c]	3.29 ± 0.77[d]	4.3 ± 0.9[e]	$5.9^{+6.1}_{-3.0}$ [f]	6.8 ± 1.2[h]	0.31 ± 0.16[i]
Br/O ($\times 10^{-6}$)	1 − 7 (2.5)		0.68 ± 0.02[d]			1.4 ± 0.3[h]	1.2 ± 0.4[i]

(a) C/2009 P1 (Garradd) from Bockelée-Morvan et al. (2014), (b) C/1995 O1 Hale-Bopp from Lis et al. (1997), (c) 103P/Hartley 2 from Bockelée-Morvan et al. (2014), (d) Early Sun from Lodders (2010), (e) HII regions from Bockelée-Morvan et al. (2014) based on GarciaŘRojas & Esteban (2007), (f) Sunspots from Bockelée-Morvan et al. (2014) based on Hall & Noyes (1969), (g) Sunspots from Bockelée-Morvan et al. (2014) based on Hall et al. (1972), (h) CI chondrites derived from Lodders (2010), (i) Earth derived from Allègre et al. (2001).

Table 4. Isotopic ratios for various solar system bodies

	67P coma	Early Sun	Vesta	Moon	Mars	Chondrites	Earth
$^{37}Cl/^{35}Cl$	0.29 ± 0.02[a]	0.3198[e] 0.31 ± 0.01[f]	0.3196-0.3207[g]	0.3198–0.3222[h]	0.3195–0.3197[i] 0.3180–0.3196[j]	0.3193–0.3197[k]	0.3200[m] 0.3197[n] 0.3196[o]
$^{81}Br/^{79}Br$	0.92 ± 0.08[b] 1.09 ± 0.16[c] 0.95 ± 0.07[d]	0.9279[e]				0.9445–0.9826[l]	0.9728[m] 0.9729[p]

(a) Average from the ^{35}Cl and ^{37}Cl fragment abundances; the uncertainty is the 1σ margin on the average, (b) Average from the $H^{79}Br$ and $H^{81}Br$ fragment abundances; the uncertainty is the 1σ margin on the average, (c) Average from the ^{79}Br and ^{81}Br fragment abundances; the uncertainty is the 1σ margin on the average, (d) Weighted average of (b) and (c), (e) Early Sun value from Lodders (2010), (f) Protostellar core value in present-day molecular clouds in the local galactic environment from Kama et al. (2015), (g) Range for volatiles in apatite in meteorites believed to be from Vesta, values from Barrett et al. (2016), (h) Range for lunar mare material collected by Apollo, and for lunar meteorites (Barrett et al. (2016), Boyce et al. (2015), Shearer et al. (2014)), (i) Range for Martian meteorites from Sharp et al. (2014), (j) Range for rocks in Gale crater analysed by NASA's Curiosity rover (Farley et al. 2016), (k) Range of values for carbonaceous, ordinary, and enstatite chondrites from (Sharp & Draper 2013), (l) Range for stony meteorites from (Wyttenbach et al. 1965), (m) Average from measurements in a variety of terrestrial reservoirs (de Groot 2009a,b), (n) NIST Standard Reference Material 975, (o) Standard Mean Ocean Chlorine (SMOC), (p) NIST Standard Reference Material 977.

presented in this paper were made at the same detector gain settings). Systematic errors associated with the instrument sensitivities are thus removed by considering the ratio of the abundances of both isotopes. If the measurements of two isotopes X and Y are interpolated onto the same time scale, the isotopic ratio can be obtained from

$$r_{X/Y} = \frac{n_X}{n_Y} = \frac{c_X - b_X}{c_Y - b_Y}, \tag{3}$$

where we correct for the presence of X and Y in the background. The overall isotopic ratio is obtained from the sum of all time-correlated measurements of isotope X divided by the sum of all time-correlated measurements of isotope Y. The uncertainty is obtained by error propagation.

The isotopic ratio for $^{37}Cl/^{35}Cl$ has been obtained from the atomic chlorine fragments in the 1–31 October 2014 period (Fig. 6, top). The elemental $^{81}Br/^{79}Br$ ratio is obtained from a weighted average of the $H^{81}Br/H^{79}Br$ (Fig. 6, bottom) and $^{81}Br/^{79}Br$ (not shown) ion fragment ratios (sufficient signal only for the 18–28 October 2014 period). An isotopic ratio of 0.29 ± 0.02 is obtained for $^{37}Cl/^{35}Cl$ and of 0.95 ± 0.07 for $^{81}Br/^{79}Br$. A comparison with the values for other solar system objects is presented in Table 4. It turns out that these values are compatible with those for the early

Sun, Earth, Moon, Mars, asteroids, and meteorites, within the measurement uncertainties.

5   HALOGENS IN REFRACTORY COMET MATERIAL

While ROSINA gives insights on the composition of the volatile fraction, Rosetta's dust composition instrument COSIMA (COmetary Secondary Ion Mass Analyzer, Kissel et al. (2007)) provides complementary information on the presence of halogens in refractory dust grains.

5.1   COSIMA operating principle

COSIMA is designed to capture and image cometary dust particles and determine the composition of their top surface layers by time-of-flight secondary ion mass spectrometry. The instrument is provided with 24 target assemblies of 3 targets covered with gold, silver, palladium, or platinum, each $10\,mm \times 10\,mm$ in size to capture dust particles. COSIMA can expose each target assembly and collect cometary dust particles at low velocity (a few m·s^{-1}) to preserve their integrity. Images of the particles are taken
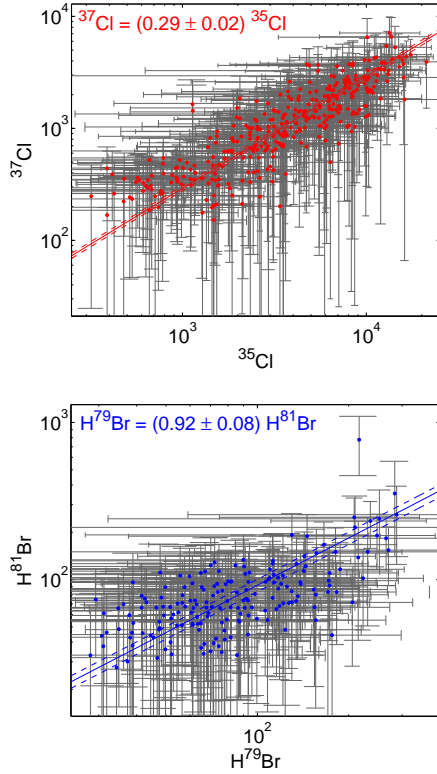
Figure 6. Chlorine and bromine isotopes. Correlating the abundances of the ^{37}Cl and ^{35}Cl fragments (1–31/10/2014) and of the H^{79}Br and H^{81}Br fragments (19–29/10/2014) provides the corresponding isotopic ratios. The error margins reflect the Poisson uncertainties. Uncertainties on the sensitivities would systematically shift the data by nearly equal amounts on both axes, so that the isotopic ratio would remain unaffected. Additional uncertainty due to the interpolation of the measurements to a common time scale has not been included in the error bars, but such errors are limited as spectra for the corresponding isotopes are acquired with little time delay.

Table 5. Dust particle over target substrate (ON/OFF particle) ratios for each peak of halogen species. The ON and OFF abundances are normalized to 75PDMS.

	$\frac{I_X}{I_{75PDMS}}$ ON	$\frac{I_X}{I_{75PDMS}}$ OFF	ON / OFF
F$^-$	14.12 ± 0.71	6.33 ± 0.45	2.23 ± 0.27
^{35}Cl$^-$	1.42 ± 0.09	1.59 ± 0.12	0.89 ± 0.12
^{37}Cl$^-$	0.39 ± 0.03	0.46 ± 0.04	0.85 ± 0.14
^{79}Br$^-$	0.23 ± 0.02	0.40 ± 0.04	0.57 ± 0.11
^{81}Br$^-$	0.11 ± 0.01	0.15 ± 0.01	0.71 ± 0.12

and specific particles are selected for analysis. During analysis, the cometary particle (and/or target plate material) is sputtered by means of an indium primary ion beam. COSIMA can be operated to collect either positive or negative secondary ions from the sputtered surface. Depending on the sampled spot, individual mass spectra may contain secondary ions from the cometary particle, the target surface, or both.

5.2 Dust particle 3D0-Kerttu

We will focus on the dust particle 3D0-Kerttu, which was collected between 18 and 24 October 2014 (period A) on a porous gold substrate. The sample temperature was about 283 K. Halogens have been observed as negative secondary ions. The secondary ions are emitted from the area analyzed by the primary indium ion beam. Due to the size of the beam and the size of the cometary particle, most of the time the mass spectra present secondary ions from the particle but also from the primary beam (^{115}In$^+$ at $m/Z = 114.90$ u/e) and from the surrounding target background, in particular gold ions at $m/Z = 196.97$ and ion fragments of a common pollutant molecule detected in TOF-SIMS experiments, PolyDiMethylSiloxane polymers (PDMS). PDMS is extremely efficiently ionized and allows the signal to be normalized using the intensity of the peak at $m/Z = 74.98$ u/e corresponding to (CH$_3$)SiO$_2^-$, a characteristic fragment of PDMS (75PDMS), in order to compare the mass spectra. To find out whether the 3D0-Kerttu dust particle contains halogens, the halogen signals relative to 75PDMS obtained on the cometary dust particle (ON particle) are compared to those measured on the target (OFF particle). Figure 7 illustrates that this comparison is conclusive only for fluorine. Table 5 gives the dust particle over target substrate (ON/OFF particle) ratios for each peak of halogen species. The ON/OFF particle ratio is greater than 1 only for fluorine. The ratios may be a bit biased due to interferences between ^{37}Cl$^-$ and C$_3$H$^-$ at nominal $m/Z = 37$ u/e, between ^{79}Br$^-$ and PO$_3^-$ at $m/Z = 79$ u/e, and between ^{81}Br$^-$ and HSO$_3^-$ at $m/Z = 81$ u/e. Analysis of more dust grains, collected in different periods, is needed to assess whether fluorine is also found in other particles, and whether chlorine and bromine are not detected at all.

6 CONCLUSIONS

We have reported the first *in situ* observations of halogens (F, Cl, Br) in a cometary atmosphere by Rosetta/ROSINA-DFMS. The main findings are

• The halogen content in the volatile fraction on 67P/C-G is mainly in the form of hydrogen halides. This result is compatible with a protosolar origin in view of our understanding of the chemical history of halogens in molecular clouds, where observations and models point to a halogen deficit in the gas phase whereas halogens end up as hydrogen halides on dust grains (Kama et al. 2015).

• The similarity of the halogen-to-oxygen element abundance ratios with the respective solar values points suggests the inclusion of the hydrogen halides into the nucleus during comet aggregation with little further evolution, if any.

• Also the isotopic composition (for the stable isotopes of chlorine and bromine) match the solar system values, further corroborating the same interpretation.

While the quantitative findings by ROSINA concerning halogens in the volatile comet material should be complemented by further evaluation of the halogens in the refractory component analysed by COSIMA, the overall conclusion is that the halogens are present at the expected abundance levels in the form of hydrogen halides, that already
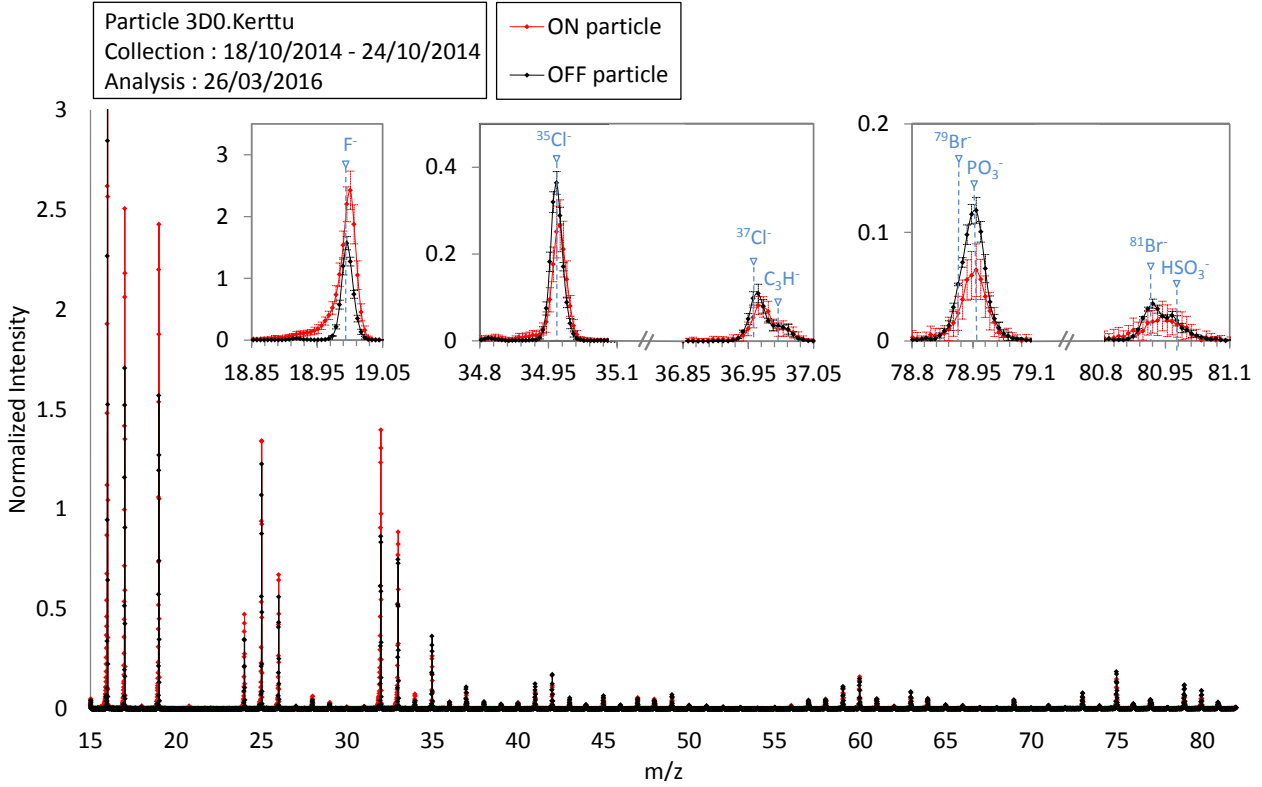
Figure 7. Halogen content on particle 3D0-Kerttu as detected by COSIMA. The particle was collected between 18 and 24 October 2014 and analyzed in March 2016. The detected halogen flux is normalized to the intensity of the $(CH_3)SiO_2^-$ fragment of the PDMS material on the target. The halogen/75PDMS ratio detected on the particle (red) and on the gold target next to the particle (black) differ significantly only for F.

froze out onto grains in the protosolar cloud and that were incorporated into the nucleus as it formed by aggregation beyond the snow line.

REFERENCES

Allègre C., Manhès G., Lewin É., 2001, Earth Planet. Sci. Lett., 185, 49

Balsiger H., et al., 2007, Space Sci. Rev., 128, 745

Balsiger H., et al., 2015, Sci. Adv., 1, e1500377

Barrett T. J., Barnes J. J., Anand M., Franchi I. A., Greenwood R. C., Charlier B. L. A., Grady M. M., 2016, in 47th Lunar Planet. Sci. Conf.. p. 2746

Bieler A., et al., 2015, Nature, 526, 678

Blake G. A., Keene J., Phillips T. G., 1985, Astrophys. J., 295, 501

Bockelée-Morvan D., et al., 2014, Astron. Astrophys., 562, A5

Boyce J. W., Treiman A. H., Guan Y., Ma C., Eiler J. M., Gross J., Greenwood J. P., Stolper E. M., 2015, Sci. Adv., 1

Calmonte U., et al., 2016, MNRAS, 462, S253

Cartwright J. A., Gilmour J. D., Burgess R., 2013, Geochim. Cosmochim. Acta, 105, 255

Dalgarno A., de Jong T., Oppenheimer M., Black J. H., 1974, Astrophys. J. Lett., 192, L37

De Keyser J., et al., 2015, Int. J. Mass Spectrom., 393, 41

De Keyser J., et al., 2017, MNRAS, this issue

Emprechtinger M., Monje R. R., van der Tak F. F. S., van der

Wiel M. H. D., Lis D. C., Neufeld D., Phillips T. G., Ceccarelli C., 2012, Astrophys. J., 756, 136

Farley K. A., et al., 2016, Earth Planet. Sci. Lett., 438, 14

GarciaŘRojas J., Esteban C., 2007, Astrophys. J., 670, 457

Hall D. N. B., Noyes R. W., 1969, Astrophys. Lett., 4, 143

Hall D. N. B., Noyes R. W., Ayres T. R., 1972, Astrophys. J., 171, 615

Hässig M., et al., 2015, Science, 347, aaa0276

Jura M., 1974, Astrophys. J., 190, L33

Kama M., et al., 2015, Astron. Astrophys., 574, A107

Kissel J., et al., 2007, Space Sci. Rev., 128, 823

Le Roy L., et al., 2015, Astron. Astrophys., 583, A1

Lis D. C., et al., 1997, Earth Moon Planets, 78, 13

Lodders K., 2010, in Goswami A., Reddy B. E., eds, , Princ. Perspect. Cosmochem.. Springer-Verlag, Chapt. 8, pp 379–417

Ménard J. M., Caron B., Jambon A., Michel A., Villemant B., 2013, in Lunar and Planetary Science Conference. p. 2375

Neufeld D. A., Wolfire M. G., 2009, Astrophys. J., 706, 1594

Neufeld D. A., et al., 2010, Astron. Astrophys., 518, L108

Peng R., Yoshida H., Chamberlin R. A., Phillips T. G., Lis D. C., Gerin M., 2010, Astrophys. J., 723, 218

Schläppi B., et al., 2010, J. Geophys. Res., 115, A12313

Sharp Z. D., Draper D. S., 2013, Earth Planet. Sci. Lett., 369-370, 71

Sharp Z., Shearer C., Burger P., Agee C., McKeegan K., 2014, in 45th Lunar Planet. Sci. Conf.. p. 1617

Shearer C. K., Sharp Z. D., Burger P. V., McCubbin F. M., Provencio P. P., Brearley A. J., Steele A., 2014, Geochim. Cosmochim. Acta, 139, 411

Squyres S. W., et al., 2012, Science, 336, 570

Vinodkumar M., Dave R., Bhutadia H., Antony B. K., 2010, Int. J. Mass Spectrom., 292, 7

Wyttenbach A., Von Gunten H. E., Scherle W., 1965, Geochim. Cosmochim. Acta, 29, 467

de Groot P. A., 2009a, in , Handb. Stable Isot. Anal. Tech. Vol. 2. Elsevier, Amsterdam, pp 721–722

de Groot P. A., 2009b, in , Handb. Stable Isot. Anal. Tech. Vol. 2. Elsevier, Amsterdam, p. 741